J. Phys. B: At. Mol. Opt. Phys. **41** (2008) 245202 (9pp) doi:10.1088/0953-4075/41/24/245202

Screening-corrected electron impact total and ionization cross sections for boron trifluoride (BF_3) and boron trichloride (BCl_3)

Minaxi Vinodkumar[1], Kirti Korot[1], Chetan Limbachiya[2] and Bobby K Antony[3]

[1] V. P. & R. P. T. P. Science College, Vallabh Vidyanagar-388 120, Gujarat, India
[2] P. S. Science College, Kadi-382 715, Gujarat, India
[3] Department of Applied Physics, ISM University, Dhanbad-826004, Jharkhand, India

E-mail: minaxivinod@yahoo.co.in

Received 6 August 2008, in final form 10 November 2008
Published 1 December 2008
Online at stacks.iop.org/JPhysB/41/245202

Abstract

In this paper, we report modified calculations for total elastic, total ionization and total (complete) cross sections for boron trifluoride (BF_3) and boron trichloride (BCl_3) upon electron impact at energies from around threshold to 2000 eV. We have proposed a model which allows screening correction due to the overlapping of atoms as seen by incident electrons in a complex molecule. We have employed the well-known spherical complex optical potential (SCOP) formalism to evaluate total elastic and total inelastic cross sections and hence total (complete) cross sections. The ionization cross sections were derived using the complex optical potential–ionization contribution (CSP-ic) method developed by us. The present results are compared with available experimental and other theoretical data wherever available and overall good agreement is observed. The present screening-corrected model shows improvement over the previous method especially at low energies. We also predict total elastic cross sections for these targets using this method.

(Some figures in this article are in colour only in the electronic version)

1. Introduction

Electron–molecule collision cross sections are increasingly important for modelling and controlling discharge environments in low-temperature plasma reactors. The driving mechanism in these plasmas is closely related to general electron–molecule scattering phenomena that occur in the precursor gases during the discharges [1]. In fact, the active fragments such as ions, radicals and atoms that are generated when electrons hit the molecular systems are responsible for several chemical reactions, such as etching, coating, polymerization, etc, leading to modification of the surface and hence the characteristics of the material. In addition, the ionization of a molecule on electron impact is a very fundamental and important collision process. Electron impact ionization cross sections find practical applications in many branches of science, e.g. fusion edge plasmas, gas discharge plasmas, planetary, stellar and cometary atmospheres, radiation chemistry, mass spectrometry and chemical analysis [2]. Despite this fact, the data concerning electron–molecule collision cross sections such as elastic, inelastic, ionization, etc are still very modest in the case of present targets. Hence, we are motivated to calculate various total cross sections (TCS) for these targets to bridge the gap between theoretical and experimental data.

The halogen-containing gases such as boron halides (BF_3, BCl_3) play a vital role in the development of plasma-assisted fabrication of microcircuits, semiconductor and telecommunication industries. BF_3 and BCl_3 are of great importance in chemical physics due to their nonpolar and

highly plane symmetric (D_{3h}) geometry. BF_3 and BCl_3 are the major sources of reactive radicals generated by electron impact dissociative processes, including electron attachment. For this reason, BCl_3 is extensively used in plasmas for the commercial etching of various semiconductors, metal surfaces [3–5] and in deposition and doping of boron [6]. The modelling of such plasmas is a challenging task, made even more difficult due to the scarcity of data on basic atomic and molecular processes involving BCl_3 and its fragments. BF_3 is also of considerable interest in chemical physics and has been widely employed as a counter gas in neutron dosimeters. It is primarily used in neutron counters [7, 8] while more recently, it has been considered as the alternative agent for plasma doping and for metal surface treatment. Moreover, it has been used as a boron source for ion implantation [9, 10].

Due to the highly reactive nature, corrosiveness and complex nature of impurities present in these boron halides, it is very difficult to handle them in scattering experiments, especially those with crossed beam techniques [5]. Hence, the experimental investigations are few compared to theoretical investigations.

BF_3 has been investigated in a variety of electron impact experiments, but there are very few results concerning electron–molecule collision cross sections. Kurepa *et al* [11] have measured the absolute total ionization and dissociative attachment cross sections for BF_3 from 16 to 250 eV. Electron attachment cross sections are also due to an earlier work given in [12, 13]. Theoretical ionization cross sections on e–BF_3 are reported by Probst *et al* [14] using the Deutsch and Märk (DM) formalism and modified additivity rule (MAR), by Kim *et al* [15] using the binary encounter Bethe (BEB) formalism and also by Huo and co-workers [16]. There is scarcity of experimental data on TCS of BF_3 and the only data reported are by Szmytkowski *et al* [17]. They have measured TCS using a linear transmission method and have reported them in the energy range from 0.6 to 370 eV.

The most detailed experimental study of electron impact partial and total ionization cross sections of BCl_3 was conducted by Jiao *et al* [18] using Fourier transform mass spectrometry in the energy range of 10–60 eV. Probst *et al* [14] employed the DM formalism and MAR method to calculate ionization cross sections for BCl_3. Kim *et al* [15] and Huo and co-workers [16] have calculated ionization cross sections for BCl_3 using BEB and siBED methods respectively for many radicals including BCl_3 from threshold to 10 keV. However, there is a paucity of experimental data on TCS for e–BCl_3 and the only available measurements are reported by Domaracka *et al* [19]. They have measured TCS using a linear transmission method and have reported in the energy range from 0.6 to 370 eV. Theoretical data on total elastic cross sections of BCl_3 are reported by Bettega [20] using the Schwinger multi-channel method with pseudo potentials at low impact energies.

2. Theoretical methodology

The 100% additivity rule (AR) also called the independent atom model (IAM) is the simplest and successful model at high energies for calculating TCS on electron impact. This model substitutes the molecules by their constituent atoms and such a crude approximation results in overestimating cross sections particularly at low energies below 100 eV. This overestimation in molecular cross section can be attributed to two facts: first, the close packed molecule is not fully transparent for low energy electrons ($E_i \lesssim 100$ eV) and, second, the mutual overlapping by neighbouring atoms is ignored; as a result the inner atoms are partially screened by the outer atoms [21]. The inclusion of the 'screening effect' leads to a decrease in molecular scattering cross section than that predicted by 100% AR. However, incorporation of the screening effect at the molecular level is difficult theoretically. Many attempts have been carried out to extend the validity of AR at low energies. Joshipura and Vinodkumar [22] separated long-range polarization potential and treated it at a molecular level and obtained cross sections from the remaining short-range interactions. Then, the TCS were evaluated adding cross sections resulting from both short-range and long-range potentials, and thus, 100% AR was modified. Bobeldijk and co-workers [23] considered the shielding effects due to the geometry of the molecule and presented a geometric additivity rule (GAR). Deutsch and co-workers [24] approximated the geometric shielding by multiplying the ionization cross sections of a cluster obtained through 100% AR by 0.5. More recently, Blanco and Garcia [25] proposed a procedure that allows correction for the overlapping of several atoms in complex molecules using AR. As an improvement over the AR method to have a better physical picture of the molecule, the single centre approximation has been used by the authors for a long time [26–32]. However, due to the overlapping of atoms in the molecule, the cross sections obtained by this method were overestimated. In the present paper, we consider BF_3 and BCl_3 molecules which are trigonal planer (see figure 1), and the central boron atom is partially shielded due to the overlapping of neighbouring fluorine or chlorine atoms, which means that the central atom is not exposed to the entire flux of incoming electrons. In other words, the central atom is 'shadowed' by other atoms surrounding it. This 'shadowing effect' is referred to as 'geometrical screening' [25]. A realistic account of such an effect through quantum mechanical treatment in terms of interaction potential is a tedious task. However, such an effect has been directly accounted for at the cross-section level. Such an attempt has been made earlier by Blanco and Garcia [25] in their IAM. The same idea has been modified and extended

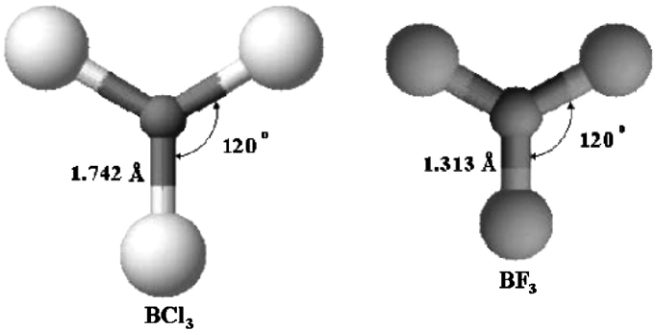

Figure 1. Structural diagram of BCl_3 and BF_3 molecules.

to our single centre approach. Because of this 'shadowing effect' or 'geometrical screening', there is a decrease in the total cross section. In the present work, we have rectified the final TCS by subtracting the cross sections arising due to the mutual overlap of the surrounding atoms with the central atom.

For many years, the spherical complex optical potential (SCOP) formalism has been successfully predicting electron impact TCS for many molecular systems. There are many modifications incorporated in the SCOP formalism such as inclusion of better charge density using standard codes and better representation of potential models. However, the basic idea of overlapping between the atoms due to the formation of the molecules is mostly overlooked. Here, we briefly describe the theoretical formalism employed in the present work to determine various TCS for the impact of electrons on the targets studied. Our aim in this paper is to calculate $Q_{\rm el}$, $Q_{\rm ion}$ and Q_T for BF_3 and BCl_3 using our new model to account for the geometrical screening correction as seen by the incident electrons. Towards this goal, we have employed the SCOP formalism, through which the total elastic cross section $Q_{\rm el}$ and its inelastic counterpart $Q_{\rm inel}$ are obtained such that

$$Q_T(E_i) = Q_{\rm el}(E_i) + Q_{\rm inel}(E_i). \tag{1}$$

The present regime of energy (ionization threshold to 2 keV) is of great significance as many scattering channels that lead to discrete as well as continuum transitions in the target are open. Therefore, we represent the electron–molecule system by a complex potential,

$$V(r, E_i) = V_R(r, E_i) + \mathrm{i}V_I(r, E_i) \tag{2}$$

such that

$$V_R(r, E_i) = V_{\rm st}(r) + V_{\rm ex}(r, E_i) + V_p(r, E_i) \tag{3}$$

where E_i is the incident energy. The three terms on the RHS of equation (3) are various real potentials arising from the electron–target interaction, namely, static, exchange and polarization potentials, respectively. All the model potentials are charge density dependent; hence, the most important basic input for evaluating all these potentials is the charge density of the target. This is obtained from the spherically averaged molecular charge density $\rho(r)$, which is determined from the constituent atomic charge densities derived from the wavefunctions of Bunge *et al* [33]. The charge density of the target is made single centre by expanding the charge density of the molecule at the centre of mass of the system. The molecular charge density, $\rho(r)$, so obtained is renormalized to incorporate the covalent bonding as in our earlier paper [27]. For the exchange potential, we have employed the parameter-free Hara 'free electron gas exchange model' [34] and for the polarization potential V_p, we have used the parameter-free model of correlation–polarization potential given by Zhang *et al* [35] which contains some multipole nonadiabatic corrections in the intermediate region and it smoothly approaches the correct asymptotic form at large r. All the target parameters, namely ionization potential, bond length and dipole polarizability of the target, used in the calculation are the best available from the literature and are given in table 1. Figure 1 shows the geometry of the BF_3 and BCl_3 molecules.

Table 1. Target properties [15, 36, 37].

Target	IP (eV)	Bond length (Å)	α_0 in a_0^3
BF_3	15.95	1.313	22.36
BCl_3	11.73	1.742	63.36

The imaginary part V_I of equation (2) consists mainly of the absorption potential $V_{\rm abs}$, which accounts for the total loss of scattered flux into all the allowed electronic channels of excitation and ionization. Here we have neglected the nonspherical terms arising from the vibrational and rotational excitation in the full expansion of the optical potential. This is due to the fact that anisotropic contribution from vibrational excitation will be significant at very low impact energies while it will be negligible at the energies of present interest. Moreover, there is no contribution from rotational excitation since these radicals do not possess permanent dipole moment due to their high symmetry.

Finally, for the absorption potential we have employed a well-known quasi-free model form of Staszewska *et al* [38] given by

$$V_{\rm abs}(r, E_i) = -\rho(r)\sqrt{\frac{T_{\rm loc}}{2}} \cdot \left(\frac{8\pi}{10k_F^3 E_i}\right) \times \theta\left(p^2 - k_F^2 - 2\Delta\right) \cdot (A_1 + A_2 + A_3). \tag{4}$$

The local kinetic energy of the incident electron is

$$T_{\rm loc} = E_i - (V_{\rm st} + V_{\rm ex}). \tag{5}$$

The absorption potential is not sensitive to long-range potentials like $V_{\rm pol}$. In equation (4), $p^2 = 2E_i$, $k_F = [3\pi^2\rho(r)]^{1/3}$ is the Fermi wave vector and Δ is an energy parameter. Further, $\theta(x)$ is the Heaviside unit step function, such that $\theta(x) = 1$ for $x \geqslant 0$, and is zero otherwise. The dynamic functions A_1, A_2 and A_3 occurring in equation (4) depend differently on $\rho(r)$, I, Δ and E_i. The energy parameter Δ determines a threshold below which $V_{\rm abs} = 0$, and the ionization or excitation is prevented energetically. In fact, Δ is the governing factor which decides the values of total inelastic cross section and that is one of the characteristics of the Staszewska model [38]. We have modified the original model by considering Δ as a slowly varying function of E_i around I. The justification for the same is discussed by Vinodkumar *et al* [30, 31]. Briefly, a preliminary calculation for $Q_{\rm inel}$ is done with a fixed value $\Delta = I$. From this the value of incident energy at which our $Q_{\rm inel}$ reaches its peak, named as E_p, is obtained. This is meaningful since Δ fixed at I would not even allow excitation at incident energies $E_i \leqslant I$. The modification introduced in our paper has been to assign a reasonable minimum value $0.8I$ to Δ and express this parameter as a function of E_i around I as follows:

$$\Delta(E_i) = 0.8I + \beta(E_i - I). \tag{6}$$

For most of the molecules, adiabatic ionization potentials are easily available. However, adiabatic ionization potentials

are not associated with the specific molecular orbital but with the appearance of specific ion products, while the vertical ionization potentials which are difficult to obtain for many cases are associated with the individual molecular orbital in the ground state of a neutral atom. Further, Kim *et al* [39] have argued that the adiabatic ionization potential and vertical ionization potential differ by about ∼1 eV or more. Vertical ionization potential is always greater than adiabatic ionization potential [40]. So for the cases where vertical ionization potential is available, β is then obtained by requiring that $\Delta = I$ (eV) at $E_i = E_p$, and also beyond E_p it is held constant equal to I. But for the molecules where vertical ionization potential is not available, β is obtained by requiring that $\Delta = I + 1$ (eV) at $E_i = E_p$, beyond which Δ is held constant equal to I. In the present case, we have taken $\Delta = I$ (eV) for evaluation of β, as vertical ionization potentials are available for both the molecules [37]. The expression for $\Delta(E_i)$, equation (6), is meaningful since Δ fixed at I would not allow excitation at incident energy $E_i \leqslant I$. On the other hand, if the parameter Δ is much less than the ionization threshold, then $V_{\rm abs}$ becomes substantially high near the peak position. After generating the full complex potential given in equation (2), we solve the Schrödinger equation numerically using partial wave analysis to get complex phase shifts that are used to find cross sections given in equation (1).

As discussed earlier, it is well evident that most of the previous methods like AR and MAR overestimated electron impact cross sections because of its inability to account for the overlapping of atoms in molecules. Even though the single centre approach developed later could largely reduce overestimation, the effect of overlapping was neglected. In the present work, we introduce a modification to the previous SCOP and complex scattering potential–ionization contribution (CSP-ic) approach. Here we calculate screening-corrected total cross section by eliminating the contribution of average screening by the surrounding atoms on the central atom within a single centre approach. A similar attempt has been made earlier by Blanco and Garcia [25], where screening correction due to the partial overlapping of atoms in a molecule was calculated using an IAM. However, in the present work, we have reduced our system to single centre, and hence the average screening effect is calculated between the central atom and the surrounding atoms, as both the targets are trigonal planar. This overlapping contribution reduces the calculated TCS.

It has to be noted that we have calculated all the cross sections, namely total elastic, total inelastic, total ionization and total (complete) cross sections without introducing the geometric screening correction as in our earlier papers [26–32] and have maintained the same symbols. In the present model, we would subtract the cross sections arising due to the 'shadowing effect' of the surrounding atom to the central atom and consider the screening-corrected total cross section of the single centre molecule given by

$$Q_{T,\rm SC} = Q_T - Q_{\rm OC}^{\rm atom} \tag{7}$$

where $Q_{T,\rm SC}$ stands for the screening-corrected TCS for the molecule, Q_T is the total cross section calculated by the single centre approach and $Q_{\rm OC}^{\rm atom}$ represents the average overlap resulting from the surrounding atoms with the central atom. We shall first show that these average pair overlapping can be approximated as $Q_{\rm OC}^{\rm atom} = Q_i Q_j/\alpha_{ij}$, where Q_i and Q_j are TCS arising due to individual the ith and jth atoms, r_{ij} is the distance between the ith and jth atoms and $\alpha_{ij} = \max\left(4\pi r_{ij}^2, Q_i, Q_j\right)$ [25].

Now, consider two atoms which are separated by a distance r_d from the centre of each atom, and the TCS resulting due to their independent existence be Q_1 and Q_2. In order to estimate the all-orientation average screening of the first atom on the second, we can imagine that the Q_1 area is spread over the total surface area $4\pi r_d^2$. Hence, $\frac{Q_1}{4\pi r_d^2}$ fraction of the first atom shadows the second atom; as a result that fraction of the second atom is not exposed to the incident flux, or in other words, $\frac{Q_1}{4\pi r_d^2}$ fraction of the second atom is not accessible to the incident flux. Consequently, an average overlapping of approximately $Q_{\rm OC}^{\rm atom} = \left(\frac{Q_1}{4\pi r_d^2}\right) Q_2$ is to be expected. Taking the other situation into account where the two atoms are very close to one another or the $4\pi r_d^2$ surface area is comparable to their individual total atomic cross sections, the $Q_{\rm OC}^{\rm atom}$ can be approximated as $Q_{\rm OC}^{\rm atom} = \min(Q_1, Q_2)$ [25]. So, in general, the averaged screened cross section arising due to the overlap or shadow effect is given by

$$Q_{\rm OC}^{\rm atom} = \frac{Q_1 Q_2}{\max\left(4\pi r_d^2, Q_1, Q_2\right)}. \tag{8a}$$

Now, we consider the present case of the trigonal planar molecules BF_3 and BCl_3. The overlap contribution is calculated between the three fluorine or chlorine atoms with the central boron atom. The central boron and surrounding halogen atoms are separated by a distance r_d and the TCS due to their independent existence being Q_1 and Q_2. Now, in the present case with a single centre approach, the $Q_{\rm OC}^{\rm atom}$ can be approximated as

$$Q_{\rm OC}^{\rm atom} = \frac{1}{N}\sum_i^N \frac{Q_i^{\rm atom} Q_c^{\rm atom}}{\alpha_{ic}}, \qquad \text{with}$$

$$\alpha_{ic} = \max\left(4\pi r_{ic}^2, Q_i^{\rm atom}, Q_c^{\rm atom}\right). \tag{8b}$$

Here N represents the total number of atoms excluding the central atom, $Q_c^{\rm atom}$ and $Q_i^{\rm atom}$ are the electron impact atomic cross sections for the pair formed by the central atom and the ith surrounding atom respectively and r_{ic} represents the bond distance between them. This reformation takes care of the average overlap contribution and gives a better representation at the lower energy regime. Also, it will partially take care of the overestimation of cross sections calculated within a single centre approach reported here. It should be noted that the present screening correction does not take into account any molecular symmetry. Hence, the present modification requires only the bond distance and atomic cross sections of individual atoms, and hence may be applied to any other larger complex molecule with ease.

Using equation (7), the expressions for the screening corrected total and inelastic cross sections are respectively given by

$$Q_{T,\mathrm{SC}} = Q_T - Q^{\mathrm{atom}}_{T,\mathrm{OC}} \quad (9)$$

$$Q_{\mathrm{inel,SC}} = Q_{\mathrm{inel}} - Q^{\mathrm{atom}}_{\mathrm{inel,OC}} \quad (10)$$

where $Q^{\mathrm{atom}}_{T,\mathrm{OC}}$ and $Q^{\mathrm{atom}}_{\mathrm{inel,OC}}$ represent the average overlap correction for total and inelastic cross sections resulting from the atomic pair with the central atom.

$Q_{T,\mathrm{SC}}$ is a measurable quantity and can have a direct comparison with the available experimental data, whereas $Q_{\mathrm{inel,SC}}$ cannot be obtained directly from experiments. The measurable quantity which is of far more practical importance is the total ionization cross section, Q_{ion}. Here $Q_{\mathrm{inel,SC}}$ does not take care of the rotation or vibration of the molecule, hence elastic to those processes. With this in mind, let us partition the total inelastic cross sections without (Q_{inel}) and with ($Q_{\mathrm{inel,SC}}$) overlap corrections into its main contributions, namely

$$Q_{\mathrm{inel}}(E_i) = \sum Q_{\mathrm{exc}}(E_i) + Q_{\mathrm{ion}}(E_i) \quad (11)$$

and

$$Q_{\mathrm{inel,SC}}(E_i) = \sum Q_{\mathrm{exc,SC}}(E_i) + Q_{\mathrm{ion,SC}}(E_i) \quad (12)$$

where the first term in both the above equations is the sum over total excitation cross sections for all accessible electronic transitions. Hereafter, we will use the screening corrected cross sections to explain our theoretical method, which is also applicable to our previous method. The second term is the TCS of all allowed ionization processes induced by the incident electrons. The first term arises mainly from the low-lying dipole allowed transitions for which the contributions of excitation cross sections to $Q_{\mathrm{inel,SC}}$ progressively decreases compared to the ionization cross sections with an increase in energy. This is because the peak of excitation cross sections occurs at lower energies; hence while the $Q_{\mathrm{ion,SC}}$ increases in the intermediate region $\sum Q_{\mathrm{exe,SC}}$ decreases. $Q_{\mathrm{ion,SC}}$ in equation (12) for electron impact ionization corresponds to continuum as against discrete optically allowed electronic excitation channels. Therefore, typically over 100 eV or so, ionization dominates over excitation. Thus, from equation (11),

$$Q_{\mathrm{inel,SC}}(E_i) \geqslant Q_{\mathrm{ion,SC}}(E_i). \quad (13)$$

Now, in order to extract $Q_{\mathrm{ion,SC}}$ from $Q_{\mathrm{inel,SC}}$, a reasonable approximation can be evolved by starting with a ratio function,

$$R(E_i) = \frac{Q_{\mathrm{ion,SC}}(E_i)}{Q_{\mathrm{inel,SC}}(E_i)} \quad (14)$$

such that $0 < R \lesssim 1$.

Perhaps the first ever estimate of ionization in relation to excitation processes was made by Turner *et al* [41]. They concluded from semi-empirical calculations that in gaseous water (H_2O), ionization was more probable than excitation above ~30 eV. If σ_{ion} and σ_{exc} are the cross sections of ionization and excitation respectively, then almost above 100 eV,

$$\frac{\sigma_{\mathrm{ion}}}{\sigma_{\mathrm{ion}} + \sigma_{\mathrm{exc}}} \approx 0.75. \quad (15)$$

It should be noted here that the denominator in equation (15) represents the total inelastic cross sections calculated here. Hence, this ratio is similar to the ratio defined by the authors using equation (14).

Since the usual complex potential calculations do not help in determining ionization contribution from the inelastic cross section, we have introduced a method based on equation (14). In the CSP-ic method, the energy dependence of $R(E_i)$ is given by the following relation [26–32]:

$$R(E_i) = 1 - f(U) \quad (16)$$

$$= 1 - C_1\left[\frac{C_2}{U+a} + \frac{\ln(U)}{U}\right] \quad (17)$$

where the incident energy is scaled to the ionization potential I through a dimensionless variable:

$$U = \frac{E_i}{I}. \quad (18)$$

Equation (17) involves the dimensionless parameters C_1, C_2 and a, which are determined by imposing three conditions on the function $R(E_i)$ as discussed in [29]. Specifically, we have $0 \leqslant R \lesssim 1$, such that

$$R(E_i)\begin{cases} =0 & \text{for} \quad E_i \leqslant I \\ =R_p & \text{for} \quad E_i = E_p \\ \cong 1 & \text{for} \quad E_i \gg E_p. \end{cases} \quad (19)$$

The reason for adopting a particular functional form of $f(U)$ in equation (17) can be understood as follows. As E_i increases above I, the ratio $R(E_i)$ increases and approaches 1 since the ionization contribution rises and the discrete excitation term in equation (11) decreases. Accordingly, the decrease in the function $f(U)$ must also be proportional to $\ln(U)/U$ in the high range of energy. However, the two-term representation of $f(U)$ given in equation (17) is more appropriate since the first term in the bracket ensures a better energy dependence at low and intermediate E_i. Here, $R_p = 0.7$ stands for the value of the ratio R at $E_i = E_p$. The choice of this value is approximate but physically justified. The peak position E_p occurs at an incident energy where the discrete excitation cross sections are on the wane, while the ionization cross section is rising fast, suggesting that the R_p value should be above 0.5 but still below 1. We have considered the general trend observed in well-known targets such as Ne, Ar, O_2, N_2, CH_4, etc [29, 41, 42], that near the peak of ionization, the contribution of the cross section $Q_{\mathrm{ion,SC}}$ is about 70–80% of the total inelastic cross section $Q_{\mathrm{inel,SC}}$ and this ratio increases with energy. However, the choice of R_p in equation (19) is not rigorous and it introduces uncertainty in the final results. For about two dozen atomic and molecular targets examined by us [26–32] so far, the said uncertainty is found to be within the experimental errors ~10–15% generally involved in most of the ionization measurements.

The dimensionless parameters C_1, C_2 and a involved in equation (17) reflect the properties of the target under investigation. The three conditions stated in equation (19) are used to determine these three parameters and hence the ratio R. This method is called the CSP-ic method. Having obtained $Q_{\mathrm{ion,SC}}$ through CSP-ic, the summed excitation cross sections $\sum Q_{\mathrm{exc,SC}}$ can be easily calculated using equation (12).

Table 2. Various total cross sections for BF_3 in Å^2.

E_i (eV)	Q_{ion}	$Q_{ion,SC}$	Q_{el}	$Q_{el,SC}$	Q_T	$Q_{T,SC}$
20	0.28	0.28	36.77	29.02	38.39	29.09
25	0.81	0.79	36.58	31.04	39.34	31.13
30	1.38	1.32	34.51	30.44	38.26	31.13
35	1.94	1.83	31.53	28.51	36.14	30.03
40	2.50	2.33	28.80	26.53	34.24	28.96
50	3.50	3.25	24.01	22.47	30.81	26.58
60	4.25	4.00	20.57	19.41	28.31	24.77
70	4.94	4.59	17.68	16.78	26.39	23.37
80	5.37	4.98	15.93	15.21	24.93	22.30
90	5.57	5.23	14.66	14.07	23.60	21.29
100	5.71	5.37	13.62	13.13	22.42	20.37
200	5.43	5.20	8.53	8.38	15.47	14.63
300	4.68	4.54	6.48	6.40	12.04	11.57
400	4.05	3.95	5.36	5.32	9.97	9.68
500	3.54	3.47	4.57	4.54	8.51	8.30
600	3.14	3.09	3.97	3.95	7.40	7.25
700	2.81	2.77	3.49	3.48	6.52	6.41
800	2.55	2.52	3.09	3.07	5.80	5.71
900	2.33	2.30	2.74	2.72	5.20	5.12
1000	2.14	2.12	2.42	2.41	4.67	4.61
2000	1.17	1.17	0.92	0.92	2.12	2.10

Table 3. Various total cross sections for BCl_3 in Å^2.

E_i (eV)	Q_{ion}	$Q_{ion,SC}$	Q_{el}	$Q_{el,SC}$	Q_T	$Q_{T,SC}$
15	1.08	1.07	–	–	–	–
20	3.61	3.56	58.22	50.68	65.97	55.55
25	6.19	6.01	49.88	44.49	61.09	52.06
30	8.41	8.06	42.79	38.72	56.85	48.69
35	9.82	9.29	37.62	34.49	53.35	45.92
40	10.56	10.07	33.79	31.35	50.26	43.52
50	11.56	11.01	30.74	28.97	48.26	42.47
60	11.92	11.29	26.75	25.35	44.35	39.29
70	12.07	11.39	24.13	23.01	41.39	36.97
80	11.98	11.36	22.22	21.33	38.64	34.78
90	11.87	11.19	20.39	19.64	36.46	33.04
100	11.64	11.01	19.22	18.55	34.47	31.41
200	9.30	8.98	12.70	12.41	24.40	23.01
300	7.76	7.56	9.95	9.77	19.15	18.35
400	6.65	6.46	8.08	7.96	15.81	15.29
500	5.78	5.69	6.76	6.68	13.53	13.16
600	5.14	5.02	5.80	5.74	11.81	11.53
700	4.70	4.58	5.07	5.02	10.52	10.30
800	4.24	4.19	4.50	4.46	9.46	9.28
900	3.95	3.81	4.04	4.01	8.54	8.40
1000	3.63	3.54	3.67	3.64	7.79	7.68
2000	2.25	2.18	1.87	1.86	4.17	4.14

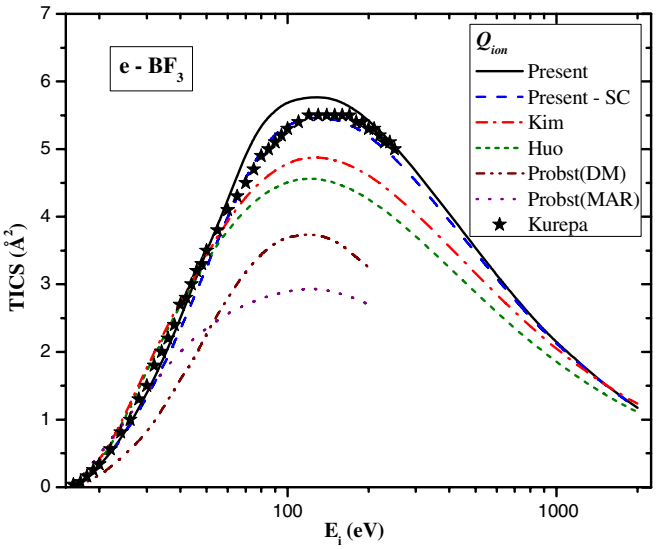

Figure 2. Total ionization cross sections for e–BF_3 scattering in Å^2. Solid line, present Q_{ion}; dashed line, present $Q_{ion,SC}$; dashed dot line, Kim *et al* [15]; short dashed line, Huo [16]; dashed dot dot line, Probst *et al* (DM) [14]; dotted line, Probst *et al* (MAR) [14]; stars, Kurepa *et al* [11].

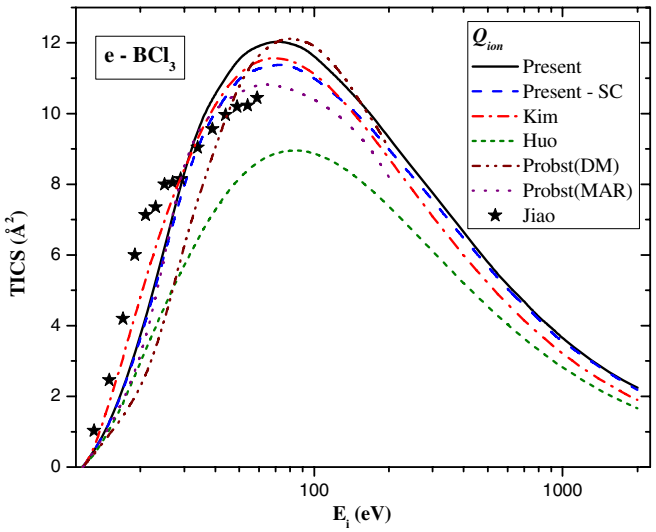

Figure 3. Total ionization cross sections for e–BCl_3 scattering in Å^2. Solid line , present Q_{ion}; dashed line, present $Q_{ion,SC}$; dashed dot line, Kim *et al* [15]; short dashed line, Huo [16]; dashed dot dot line, Probst *et al* (DM) [14]; dotted line, Probst *et al* (MAR) [14]; stars, Jiao *et al* [18].

3. Results and discussion

The theoretical approach of SCOP along with our CSP-ic method discussed above offers the determination of the total elastic cross sections, Q_{el}, $Q_{el,SC}$, total inelastic cross sections, Q_{inel}, $Q_{inel,SC}$, and total ionization cross sections, Q_{ion}, $Q_{ion,SC}$, along with a useful estimate on electronic excitations in terms of the summed cross section $\sum Q_{exc}$, $\sum Q_{exc,SC}$. The present data of total elastic, total ionization and total (complete) cross sections along with their screening corrected results for BF_3 and BCl_3 are tabulated in tables 2 and 3. Total ionization cross sections for both the targets are calculated using the CSP-ic method. Further, the present results are compared with available theoretical as well as experimental results through figures 2–5. In figure 6, we have mutually compared the total ionization and total (complete) cross sections for both halides.

BF_3 radical is more widely studied theoretically than experimentally. Figure 2 shows the comparison of present total ionization cross sections along with the overlap corrections for e–BF_3 scattering. There is a noticeable reduction in cross section due to the screening correction towards the peak and lower energy region as expected. This result seems to agree very well with the measurements of Kurepa *et al* [11]. The

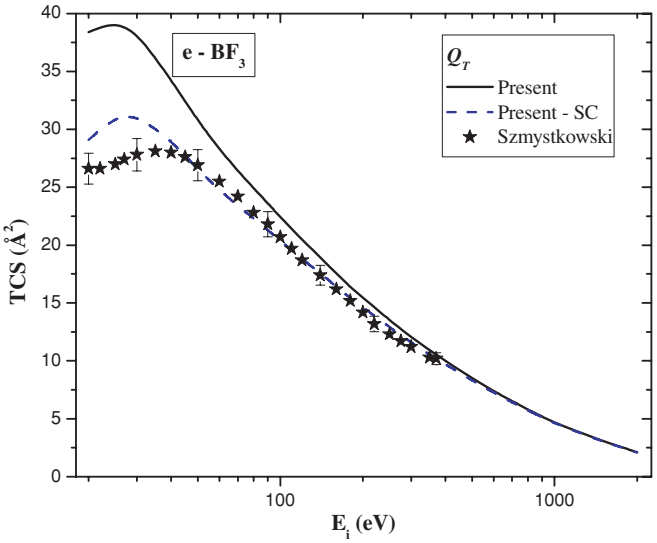

Figure 4. Total cross section for e–BF_3 scattering in Å^2. Solid line, present Q_T; dashed line, present $Q_{T,SC}$; stars, Szmytskowski *et al* [17].

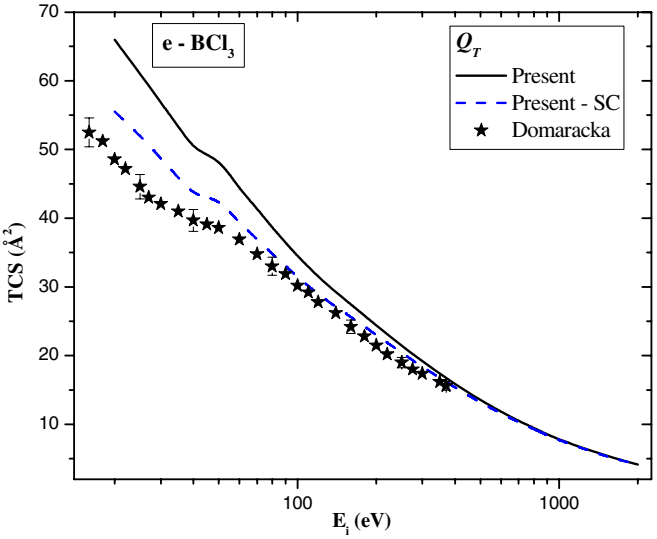

Figure 5. Total cross section for e–BCl_3 scattering in Å^2. Solid line, present Q_T; dashed line, present $Q_{T,SC}$; stars, Domaracka *et al* [19].

results of Probst *et al* [14] by the DM formalism are much lower than the present results throughout their reported energy range, while their MAR values are in agreement at lower energies, but underestimate all results presented here, at higher energies. This is a regular feature of the DM formalism as discussed in our earlier article [32]. The theoretical values of Kim *et al* [15] and Huo and co-workers [16] are lower than the present results and experimental data above 30 eV. Kurepa *et al* [11] have measured Q_{ion} for e–BF_3 only up to 250 eV. Their results are in excellent accord with the present $Q_{ion,SC}$ throughout their measured energy range.

A comparison of electron impact ionization cross sections for BCl_3 radical is presented in figure 3. The literature survey shows a similar trend as BF_3, with only one measurement out of five works presented here. The measurement from Jiao *et al* [18] is the only experimental data available from the

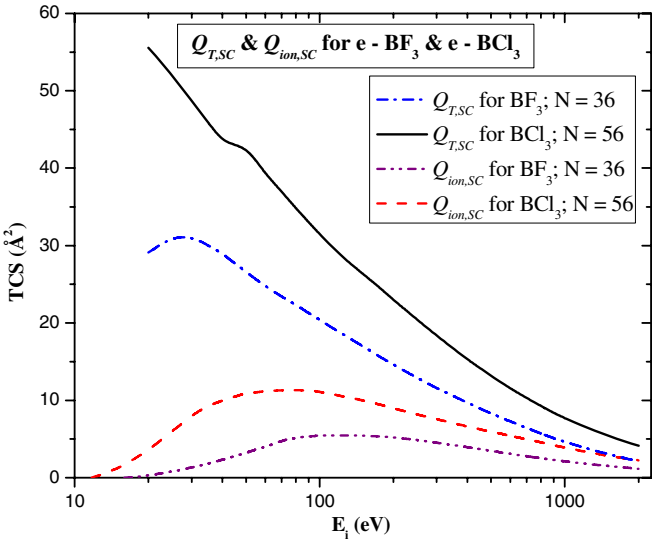

Figure 6. Comparison of $Q_{T,SC}$ and $Q_{ion,SC}$ for BF_3 and BCl_3. Dashed dot line, present $Q_{T,SC}$ for BF_3; solid line, present $Q_{T,SC}$ for BCl_3; dashed dot dot line, present $Q_{ion,SC}$ for BF_3; dashed line, present $Q_{ion,SC}$ for BCl_3.

literature, which may be attributed to its reactive nature and hence difficult to handle in laboratories. Measurement does not seem to follow the same structure as the theories in this case. At around 20 eV, it crosses over most of the theoretical values from higher to lower side. The overall comparison has a similarity with BF_3 except that the theoretical values of Probst *et al* [14] by the DM formalism are much higher here. They seem to agree with the present results from the peak and beyond. However, their MAR values are close to the present results below 30 eV and seem to agree better with the measurements than other results presented here. The theoretical values of Kim *et al* [15] agree very well with our results, while that of Huo and co-workers [16] are much lower and similar to what we observed in the case of BF_3.

Figure 4 shows the comparison of TCS of BF_3 on electron impact with available results. There are no theoretical data found in the literature in the present energy range and are hence reported for the first time. Moreover, due to its reactive nature the experimental results are also modest and the only experimental data reported are by Szmytkowski *et al* [17]. It should be noted that screening corrected TCS are lower than results without corrections, and the effect of screening is more at lower incident energies below 100 eV. Moreover, both our results with and without screening corrections merge above 300 eV. The screening corrected TCS are in excellent accord with experimental results of Szmytkowski *et al* [17] above 40 eV and below which the present values are slightly higher. Da Costa *et al* [1] have used the Schwinger multichannel method to calculate elastic integral cross sections using static-exchange potentials only up to 40 eV. Their values are lower than all presented data; however, the data are not shown in figure 4.

Figure 5 shows the comparison of the total cross section for BCl_3 on electron impact with available comparisons. As seen in BF_3, here also screening corrected TCS are lower

than results without correction and the effect of screening is more pronounce at low impact energies. In the case of BCl_3, it can also be noted that our results with and without screening corrections merge above 300 eV. The experimental as well as theoretical data for the TCS are modest. The only theoretical data reported are by Bettega [20] who have used the Schwinger multichannel method to evaluate elastic scattering of low energy electrons at the static-exchange approximation. The present screening corrected TCS are in very good accord with the experimental data of Domaraca *et al* [19] beyond 60 eV, below which they are slightly higher compared to them. There is small shoulder seen in our both the results around 40–60 eV, which is also observed in the data of Domaraca *et al* [19]. The weak shoulder spanned between 30 and 60 eV reflects the significant increase in ionization efficiency with the maximum around 60–70 eV [19]. This increase in the ionization efficiency can be attributed due to the opening of other inelastic channel with threshold around 50 eV. At this energy, there is a larger production of BCl_2^+ due to the reaction of more extensively dissociated ions BCl^+ and Cl^+ with BCl_3 to produce BCl_2^+ [18]. It is further experimentally observed by Jiao *et al* [18] that the depletion of Cl^+ is about 1.5 times faster at 50 eV, which in turn explains the increase in the production of BCl_2^+ at this energy. This enhancement in the production of BCl_2^+ increases the ionization efficiency which is well reflected as a weak shoulder in the TCS in figure 5.

Our final figure (figure 6) represents the mutual comparison of total screening corrected ionization and TCS for both the boron halides. As can be seen from the plots, both the ionization and total cross section for boron chloride are higher than those for boron fluoride. This is attributed to the bigger geometrical size of boron chloride compared to boron halide. The total cross section increases with an increase in the geometrical size of the target. The geometrical size further depends on the total number of electrons which is 36 in the case of BF_3 and 56 in the case of BCl_3. Moreover, at sufficiently high energies these cross sections for both halides merge, reflecting the fact that at high energies the time spent by the electron in the vicinity of the target decreases and hence the cross section.

4. Conclusion

Calculations employing the previous formalism (SCOP and CSP-ic) and the modified method were made for the molecular systems BF_3 and BCl_3. As we have expected, the differences between these two methods were prominent at the low energy regime. These values are reported in tables 2 and 3, respectively. The geometrical screening correction lowers the total ionization and TCS and the effect is important below 100–200 eV. The screening corrected total ionization and TCS show better agreement with available experimental and theoretical data. The complex scattering potential–ionization contribution (CSP-ic) formalism developed by the authors [26–32] is used to derive the total ionization cross section for these targets. This method has been tested successfully for a large number of atomic and molecular targets. The derived theoretical inelastic cross section serves as the upper bound and gives a useful estimation of the total ionization cross sections. We note that in view of the approximations made here, no definitive values are claimed, but by and large our results fall well within the experimental error limits in all the cases. The present theoretical results for the total ionization and TCS show very good agreement with most of other theoretical investigations. Moreover, a mutual comparison of TCS for the boron trichloride and boron trifluoride is carried out, and it reflects the fact that TCS increases with the increase in the geometrical size of the target. Also, the present method employed here provides an estimate of electronic excitations in relation to ionization cross sections in a particular target. We have not provided the data of total excitation cross sections but these are available from the authors. Finally, we hope that the present work may inspire the experimentalists as there is a paucity of experimental data for these targets.

Acknowledgments

MVK and CGL are grateful to the University Grants Commission, New Delhi, for a Major Research Project under which part of this work is carried out. The authors are grateful to Professor P C Vinodkumar, Sardar Patel University, for fruitful discussion.

References

[1] da Costa R F, Ferreira L G, Lima M A P and Bettega M H F 2003 *J. Chem. Phys.* **118** 75
[2] Märk T D and Dunn G H (eds) 1985 *Electron Impact Ionization* (Vienna: Springer)
[3] Reents W D 1986 *Anal. Chem.* **58** 2797
[4] Stockdale J A, Nelson D R, Davis F J and Compton R N 1972 *J. Chem. Phys.* **56** 3336
[5] Christophorou L G and Olthoff J K 2002 *J. Phys. Chem. Ref. Data* **31** 971
[6] Jackman R B, Baral B, Kingsley C R and Foord J S 1996 *Diamond Relat. Mater.* **5** 378
[7] Fowler I L 1963 *Rev. Sci. Instrum.* **34** 731
[8] Chen C-Y and Chung C 1997 *Nucl. Instrum. Methods Phys. Res.* A **395** 195
[9] Kruzelecky R V, Racansky D, Zukotynski S, Perz J M, Polk D and Lau W M 1986 *J. Non-Cryst. Solids* **79** 19
[10] Hunger H-J and Lobing G 1997 *Thin Solid Films* **310** 244
[11] Kurepa M V, Pejcev V M and Cadez I M 1976 *J. Phys. D: Appl. Phys.* **9** 481
[12] Chantry P J 1974 *Bull. Am. Phys. Soc.* **19** 149
[13] Harland P W and Franklin J L 1974 *J. Chem. Phys.* **61** 1621
[14] Probst M, Deutsch H, Becker K and Märk T D 2001 *Int. J. Mass Spectrom.* **206** 13
[15] From http://physics.nist.gov/PhysRefData/Ionization/molTable.html
[16] From http://www.ipt.arc.nasa.gov/databasemenu.html
[17] Szmytkowski C, Piotrowicz M, Domaracka A, Klosowski L, Denga E P and Kasperski G 2004 *J. Chem. Phys.* **121** 1790
[18] Jiao C Q, Nagpal R and Haaland P 1997 *Chem. Phys. Lett.* **265** 239
[19] Domaracka A, Ptasinska-Denga E and Szmytkowski C 2005 *Phys. Rev.* A **71** 052711
[20] Bettega M H F 2000 *Phys. Rev.* A **61** 042703
[21] Jiang Y, Sun J and Wan L 2000 *Phys. Rev.* A **62** 062712
[22] Joshipura K N and Vinodkumar M 1997 *Phys. Lett.* A **224** 361
[23] Bobeldijk M, Van Der Zande W J and Kistemaker P G 1994 *Chem. Phys.* **179** 125

[24] Deutsch H, Becker K, Pittner J, Bonacic-Koutecky V, Matt S and Märk T D 1996 *J. Phys. B: At. Mol. Opt. Phys.* **29** 5175
[25] Blanco F and Garcia G 2003 *Phys. Lett.* A **317** 458
[26] Vinodkumar M, Joshipura K N, Limbachiya C and Mason N 2006 *Phys. Rev.* A **74** 022721
[27] Vinodkumar M, Joshipura K N and Mason N J 2006 *Acta Physica Slovaca* **56** 521
[28] Vinodkumar M, Joshipura K N, Limbachiya C G and Antony B K 2006 *Eur. Phys. J.* D **37** 67
[29] Vinodkumar M, Limbachiya C, Antony B and Joshipura K N 2007 *J. Phys. B: At. Mol. Opt. Phys.* **40** 3259
[30] Vinodkumar M, Limbachiya C, Korot K, Joshipura K N and Mason N 2008 *Int. J. Mass Spectrom.* **273** 145
[31] Vinodkumar M, Limbachiya C, Korot K and Joshipura K N 2008 *Eur. Phys. J.* D **48** 333
[32] Joshipura K N, Vinodkumar M, Antony B K and Mason N J 2003 *Eur. Phys. J.* D **23** 81
[33] Bunge C F, Barrientos J A and Bunge A V 1993 *At. Data Nucl. Data Tables* **53** 113
[34] Hara S 1967 *J. Phys. Soc. Japan* **22** 710
[35] Zhang X, Sun J and Liu Y 1992 *J. Phys. B: At. Mol. Opt. Phys.* **25** 1893
[36] Lide D R 1993–94 *CRC Handbook of Physics and Chemistry* 74th edn (Boca Raton, FL: Chemical Rubber Company)
[37] From http://srdata.nist.gov/cccbdb/
[38] Staszewska G, Schwenke D W, Thirumalai D and Truhlar D G 1983 *Phys. Rev.* A **28** 2740
[39] Kim Y-K, Hwang W, Weinberger N M, Ali M A and Rudd M E 1997 *J. Chem. Phys.* **106** 1026
[40] From http://cccbdb.nist.gov/adiabatic.asp
[41] Turner J E, Paretzke H G, Hamm R N, Wright H A and Richie R H 1982 *Radiat. Res.* **92** 47
[42] Karwasz G P, Brusa R S and Zecca A 2001 *Nuovo Cimento* **24** 1